Electronic Supplementary Information

Compositional engineering of $ZnBr_2$-doped $CsPbBr_3$ perovskite nanocrystals: Insights into structure transformation, optical performance, and charge-carrier dynamics

V. Naresh [a], Kiran Gupta [b], Kyunghoon Lee [c], Jiwoong Yang [c], Pil-Ryung Cha*[,a], Nohyun Lee*[,a]

[a]School of Advanced Material Engineering, Kookmin University, Seoul 02707, Republic of Korea.

[b]Department of Chemical Engineering, Kyung Hee University, 1732 Deogyeong-daero, Giheung-gu, Yongin, Gyeonggi-do 17104, Republic of Korea.

[c]Department of Energy Science and Engineering, Daegu Gyeongbuk Institute of Science and Technology (DGIST), Daegu 42988, Republic of Korea.

*Corresponding author email: cprdream@kookmin.ac.kr (Pil-Ryung Cha), nohyunlee@kookmin.ac.kr (Nohyun Lee)

Materials and chemicals:

Lead bromide ($PbBr_2$, 99.99% Sigma-Aldrich), cesium carbonate (Cs_2CO_3, 99.99% Sigma-Aldrich), zinc bromide ($ZnBr_2$, 99.99% Sigma-Aldrich), 1-octadecene (ODE, 90% Sigma-Aldrich), oleic acid (OA, 90% Sigma-Aldrich), oleylamine (OLA, 80-90% Sigma-Aldrich), Methyl acetate (MeOAc, 99.5% Sigma-Aldrich), n-hexane (95.0% Samchun), toluene (99.99% Samchun) and Polystyrene (PS, Mw: ~350,000 by GPC, Sigma-Aldrich) were purchased and used without further purification.

Synthesis methodology:

Preparation of caesium-oleate: Cs_2CO_3 (0.4073 g, 1.25 mmol), 15 mL ODE, and 1.35 mL OA were loaded into a 100 mL 3-neck flask, heated to 120 °C under vacuum for 1 h, and then heated under Ar gas flow at 150 °C until Cs_2CO_3 was completely dissolved, and a clear solution was obtained. The Cs-oleate solution is kept at this temperature (150 °C) before

it was injected.

Synthesis of $CsPbBr_3$ perovskite NCs: $PbBr_2$ (0.138 g, 0.376 mmol) and ODE (10 mL) were loaded into a 50 mL 3-neck flask, heated to 120 °C under vacuum for 1 hr, and then followed by heating the solution to 150 °C under Ar gas. Dried OA and OAm (each 1 mL) at 100 °C were injected into the $PbBr_2$-ODE solution at 120 °C under the flow of Ar gas. After complete solubilization of $PbBr_2$ salt, the temperature was raised to 160-170 °C and kept at this temperature for 5 minutes. Then, Cs-oleate solution (0.85 mL) was swiftly injected into the $PbBr_2$-ODE solution, and after 60 s the solution was immediately cooled down to room temperature by immersing the flask in an ice-water bath.

Synthesis of $ZnBr_2$-doped $CsPbCl_3$ perovskite NCs: The procedure described above was followed for the synthesis of $ZnBr_2$-doped $CsPbCl_3$ perovskite PNCs. In this procedure, A specific amount of and 0%, 20%, 40%, 60%, 80% $ZnBr_2$ were added to the $PbBr_2$, and ODE (10 mL) were loaded into a 50 mL 3-neck flask and heated to 120 °C under vacuum for 1 h and then followed by heating the solution to 150 °C under Ar gas. Dried OA and OAm (each 1 mL) at 100 °C were injected into the $PbBr_2$-ODE solution at 120 °C under the flow of Ar gas. After complete solubilization of $PbBr_2$ salt, the temperature was raised to 175-180 °C and kept at this temperature for 5 minutes. Then, Cs-oleate solution (0.85 mL) was swiftly injected into the $PbBr_2$-$ZnBr_2$-ODE solution, and after 60 s the solution was immediately cooled down to room temperature by immersing the flask in an ice-water bath.

Purification of nanocrystals: As-synthesized $CsPbBr_3$ and $ZnBr_2$-doped $CsPbBr_3$ PNCs were extracted from the crude solution by centrifuging at 8000 rpm for 5 min and then discard the supernatant. This process was repeated for one more time by adding 4 ml MeOAc and centrifuging to remove the residual mixture. Then, the precipitate was redispersed in 2 ml MeOAc and 2 ml n-hexane and centrifuged again for 5 min at 8000 rpm, and the supernatant

was discarded. Subsequently, the particles in the centrifuge tube were dispersed again in 5 ml n-hexane and centrifuged for 5 min at 5000 rpm supernatant was discarded. Finally, the precipitate was re-dispersed in toluene (or n-hexane for optical characterization) forming stable colloidal solutions. For solid NCs powders, the precipitate obtained in the above step was dried under a vacuum at 60 °C overnight.

Synthesis of $K_2SiF_6:Mn^{4+}$ and Zn-doped $CsPbBr_3$ composite: The $K_2SiF_6:Mn^{4+}$ and Zn-doped $CsPbBr_3$ powders were weighed in the mass ratio of 0.6/ 0.4 and was homogeneously dispersed in the polystyrene-toluene solution (0.1 g of polystyrene granules and 1 mL of toluene). Subsequently, 250 µL of the dispersion was drop-casted on a quartz substrate (13 mm ×13 mm) and naturally dried for 2 hours to remove the solvent. Finally, a uniformly coated $K_2SiF_6:Mn^{4+}$/Zn-doped $CsPbBr_3$ composite film-coated glass substrate was obtained.

Fabrication of $K_2SiF_6:Mn^{4+}$/Zn-doped $CsPbBr_3$ composite film-coated WLED: A prototype white-LED device is fabricated by directly stacking the $K_2SiF_6:Mn^{4+}$/ Zn-doped $CsPbBr_3$ composite film coated glasses onto a commercially available blue-emitting InGaN LED chip (455 nm).

Characterizations.

X-ray diffraction (XRD) patterns of pristine and Zn-doped PNCs were recorded on a Bruker DE/D8 Advance X-ray Diffractometer equipped with Cu Kα (λ = 1.541 Å) radiation source operated at 60kV and 60 mA at room temperature. The samples were provided in dry powder form and scanned within the range of 2θ from 10 to 60°. The morphology of the pristine and Zn-doped PNCs was investigated from the transmission electron microscopy (TEM) and high-resolution TEM (HR-TEM) images acquired on a JEM-2100/ JEOL/ JP operated at 200 kV accelerating voltage. The 300 mesh copper Formvar/ carbon grid was dipped into the 50 µl PNCs dispersed in 1 ml of a toluene solution and allowed to dry in ambient conditions

overnight. Inductively coupled plasma-atomic emission spectroscopy (ICP-AES) characterization was carried out on a Shimadzu ICPS-8100 twin sequential high-frequency plasma emission spectrometer. The dried samples (0.055g) were first digested in warm (2% HNO_3 and 1% HCl) acid solution (~95 ℃, over a night) until completely dissolved forming a transparent liquid. The obtained solution was then diluted with deionized water, and the resultant solution was filtered through a syringe filter with 0.22 μm pore size before the analysis. The samples were measured under an N_2 atmosphere as a purging gas, ranging from 30°C to 1000 °C with a heating rate of 10 K/min. The X-ray photoelectron spectroscopy (XPS) measurement for $CsPbCl_3$ and Mn-doped $CsPbCl_3$ PNCs materials were conducted on an Ulvac PHI/X-tool spectrometer with Al Kα radiation source (1486.6 eV, 24.1W, 15kV) and a beam diameter of 100 μm×100 μm. Raman spectrum is measured using *Jobin Yvon Horiba (LABRAM HR - 800)* Micro Raman spectrometer attached with the Ar^+ laser (514.5 nm) as the excitation source having an output power of 1.2 μW, with a laser beam spot size of 100 μm. TA spectra for pristine and Zn-doped $CsPbBr_3$ PNCs were measured in the range of 430-600 nm at a pump wavelength of 400 nm and energy of ~5 nJ/pulse at different pump-probe delay times on a home built femtosecond transient absorption spectroscopy (fs-TA) setup based on a 1 kHz Ti: sapphire regenerative amplifier (Astrella, Coherent) with ~50 fs fundamental pulses at 805 nm. A sapphire window with a thickness of 2 mm was exposed to laser pluses at 800 nm, which produced white continuum light (WCL) ranging from 380 to 800 nm. The WCL was divided into two beams: one for probing and one for reference. The WCL pulses were detected with pump by using a 500 Hz mechanical chopper. All the TA measurements used a pump beam with a wavelength of 400 nm. The probe and reference beams were collected by two fiber spectrometers to record and calculated the TA dynamics. A series of PNCs toluene solutions were prepared by dispersing 0.025 mg of PNCs in 1 ml of toluene and used to conduct

absorption, PL, and time-resolved spectroscopy measurements. UV-Vis absorption spectra were measured in the range of 300-700 nm on a Shimadzu UV-2600 spectrometer. The steady-state fluorescence spectra (PL and PLE) were recorded using a Shimadzu RF-6000 Spectro-fluoro-photometer equipped with a 150 W Xe lamp as an excitation and scanning speed of 60,000 nm/min. The time-resolved decay curves of the samples were measured on a HORIBA Jobin Yvon FluoroMax-4 fluorescence spectrometer equipped with a 150 W Xe lamp as an excitation source at room temperature. The PLQY of the PNCs dispersed toluene solutions were measured by employing an integrated sphere unit attached to Shimadzu RF-6000 Spectro-fluoro-photometer according to the standard procedure using Toluene as a reference under ambient conditions. Electroluminescence spectra were measured on a Labsphere CdS-610 spectrometer.

Table S1. ICP-AES data analysis of $CsPbBr_3$:*x*%Zn PNCs with different concentrations of $ZnBr_2$ (0, 20, 40, 60, and 80%)

Doping Content of $ZnBr_2$ (%)	Zn content (at%)
0	0
20	2.52
40	4.56
60	7.03
80	8.94

Table S2. Band position and their assignment in the Raman spectra of $CsPbBr_3$ and Cs_4PbBr_6.

Sample	Band position (cm-1)	Assignment of Raman bands	Ref.
$CsPbBr_3$	129.4	- is attributed to the transverse-optical (TO) phonon mode due to symmetric stretching vibrations of the Pb-Br bonds in the octahedra	**[S1, S2]**
	160.7	- is attributed to the longitudinal-optical (LO) phonon mode due to symmetric stretching modes of Pb-Br bonds in the octahedra	**[S1, S3]**
	313.5	- is attributed to the second-order (longitudinal optical (LO)) phonon mode corresponding to the vibration of Pb-Br bond.	**[S1, S3, S4]**
Cs_4PbBr_6	114.7	- is attributed to the bending modes of the Pb-Br bonds in the octahedra	**[S1]**
	130.8	- is attributed to the transverse-optical (TO) phonon mode due to symmetric stretching vibrations of the Pb-Br bonds in the octahedra	**[S1, S2]**
	166.2	- is attributed to the longitudinal-optical (LO) phonon mode due to symmetric stretching modes of Pb-Br bonds in the octahedra	**[S1, S3]**

Table S3. XPS data analysis of $CsPbBr_3$:*x*%Zn PNCs with different concentrations of $ZnBr_2$ (0, 20, 40, 60, and 80%)

Doping Content of $ZnBr_2$ (%)	Zn content (at%)
0	0
20	1.96
40	3.3
60	6.8
80	8.2

Table S4. PLQY, decay components (τ_1 and τ_2), lifetime (τ), radiative decay rate (k_r), nonradiative decay rate (k_{nr}) of $CsPbBr_3$ and $ZnBr_2$ doped $CsPbBr_3$ PNCs.

Doping Content of $ZnBr_2$ (%)	PLQY (%)	τ_1 (ns)	τ_2 (ns)	Lifetime (± 0.1 ns)	k_r (± 0.01 ns^{-1})	k_{nr} (± 0.01 ns^{-1})	k_r/k_{nr} ± 0.01
$CsPbCl_3$	50.1	1.72	22.67	13.6	0.0368	0.0367	1.0041
20 $ZnBr_2$	62.3	7.63	25.22	16.2	0.0385	0.0233	1.653
40 $ZnBr_2$	79.8	6.70	32.85	19.8	0.0402	0.0102	3.9505
60 $ZnBr_2$	98.6	6.55	34.01	23.3	0.0424	0.00061	70.429
80 $ZnBr_2$	54.2	13.07	24.65	14.5	0.0375	0.0317	1.1834

Table S5. Temperature-dependent decay lifetimes of $CsPbBr_3$ and 60% $ZnBr_2$ doped PNCs.

Temperature (K)	$CsPbBr_3$	60% $ZnBr_2$ doped PNCs
10	4.41	9.14
50	6.18	6.20
100	6.79	9.67
150	7.48	12.48
200	9.40	14.43
250	10.81	15.3
300	11.63	17.56
350	16.12	19.58
375	11.87	24.29
400	10.05	27.52

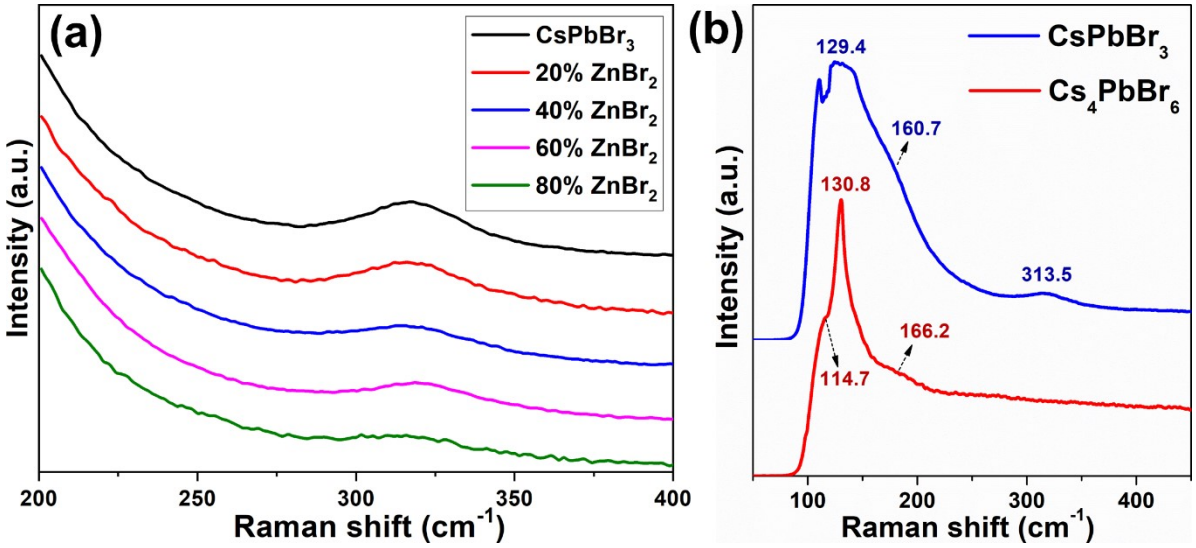

Fig. S1. Raman spectra of the (a) $CsPbBr_3$ and $CsPbBr_3$:x% $ZnBr_2$ (x = 0, 20, 40, 60, and 80%), (b) comparison of the Raman spectral profiles of $CsPbBr_3$ and Cs_4PbBr_6.

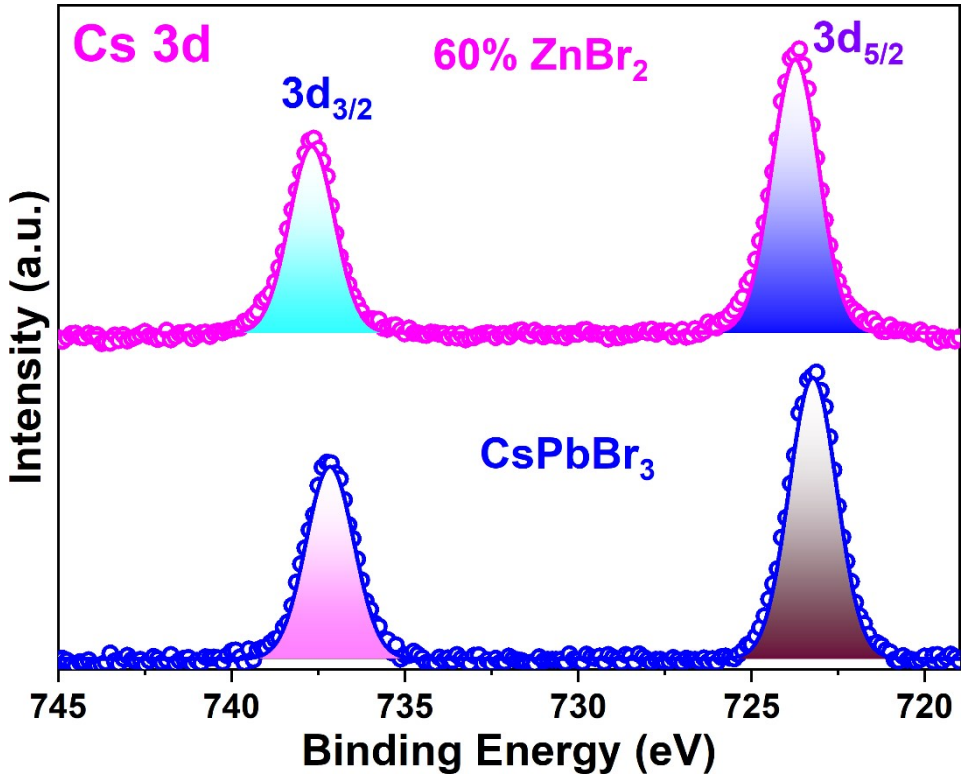

Fig. S2. Narrow-scan XPS spectrum of Cs ($3d_{3/2}$, $3d_{5/2}$) for pristine $CsPbBr_3$ and $ZnBr_2$-doped PNCs.

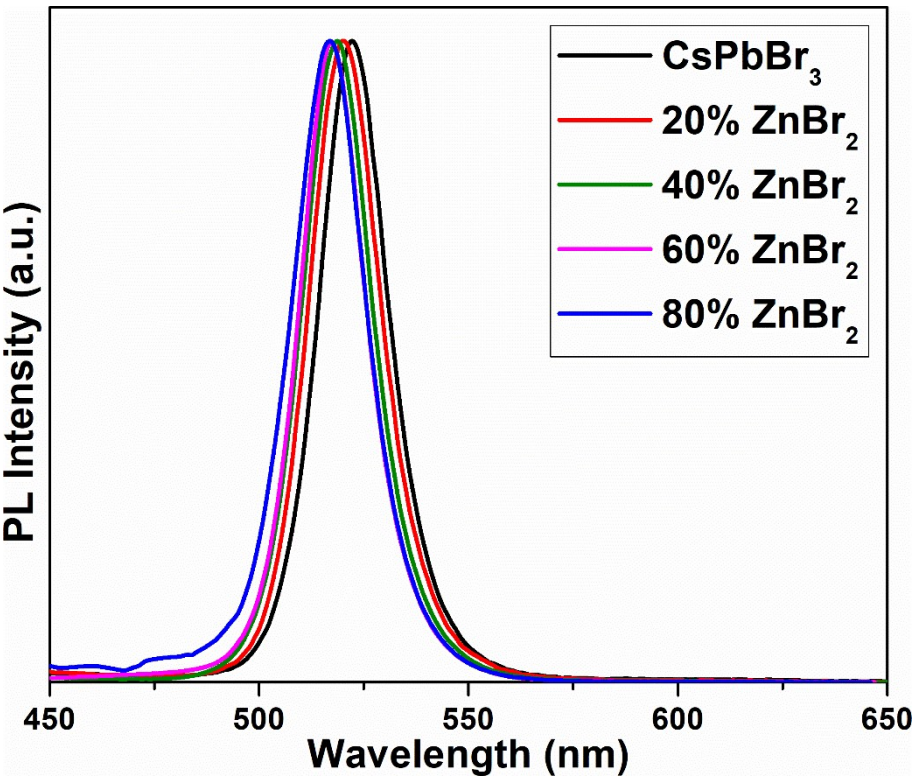

Fig. S3. Normalized PL spectra for pristine $CsPbBr_3$ and $ZnBr_2$-doped PNCs.

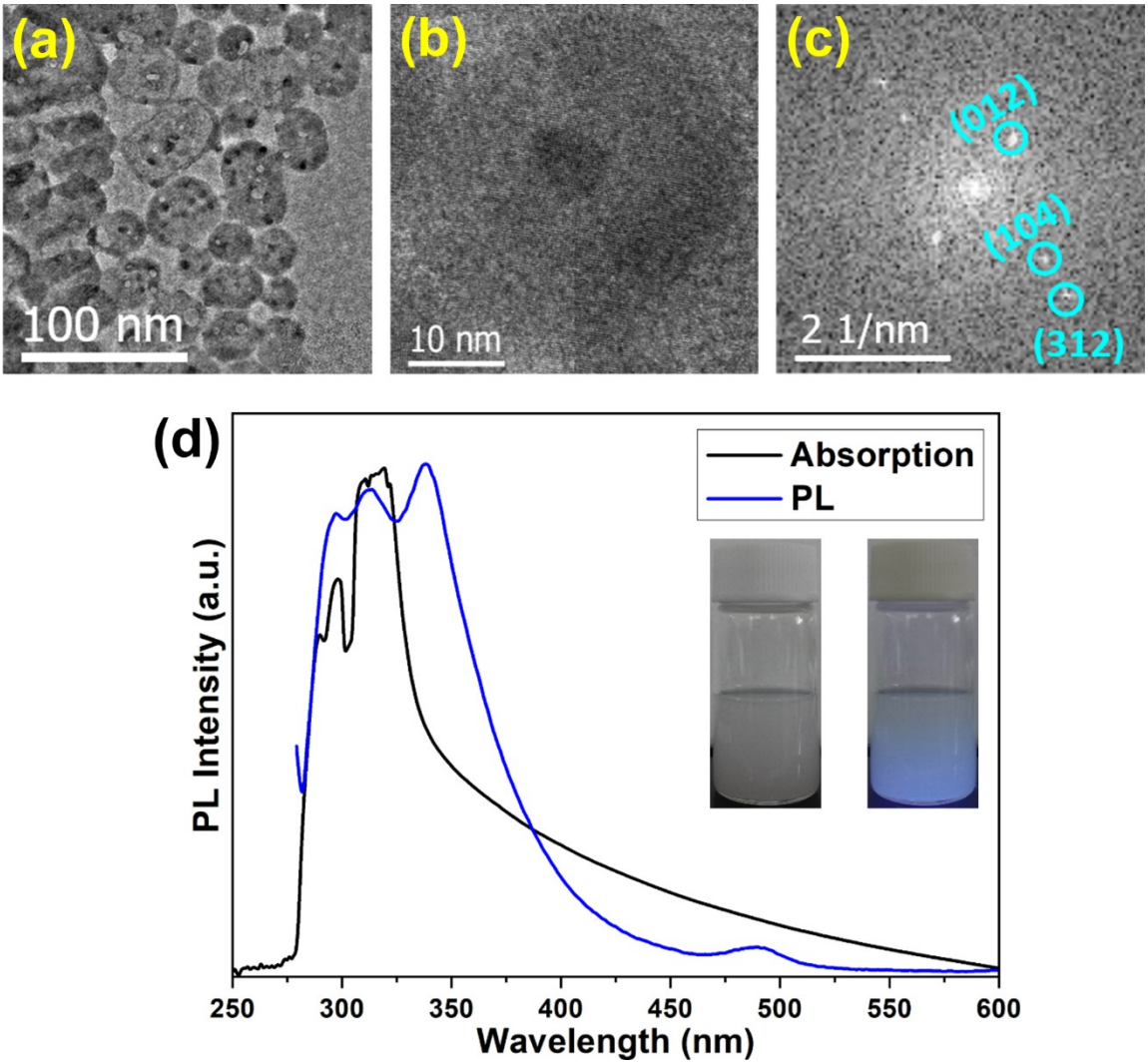

Fig. S4. (a) TEM, (b) HR-TEM and (c) corresponding FFT image, optical and luminescence properties of 96% $ZnBr_2$ doped $CsPbBr_3$ PNCs.

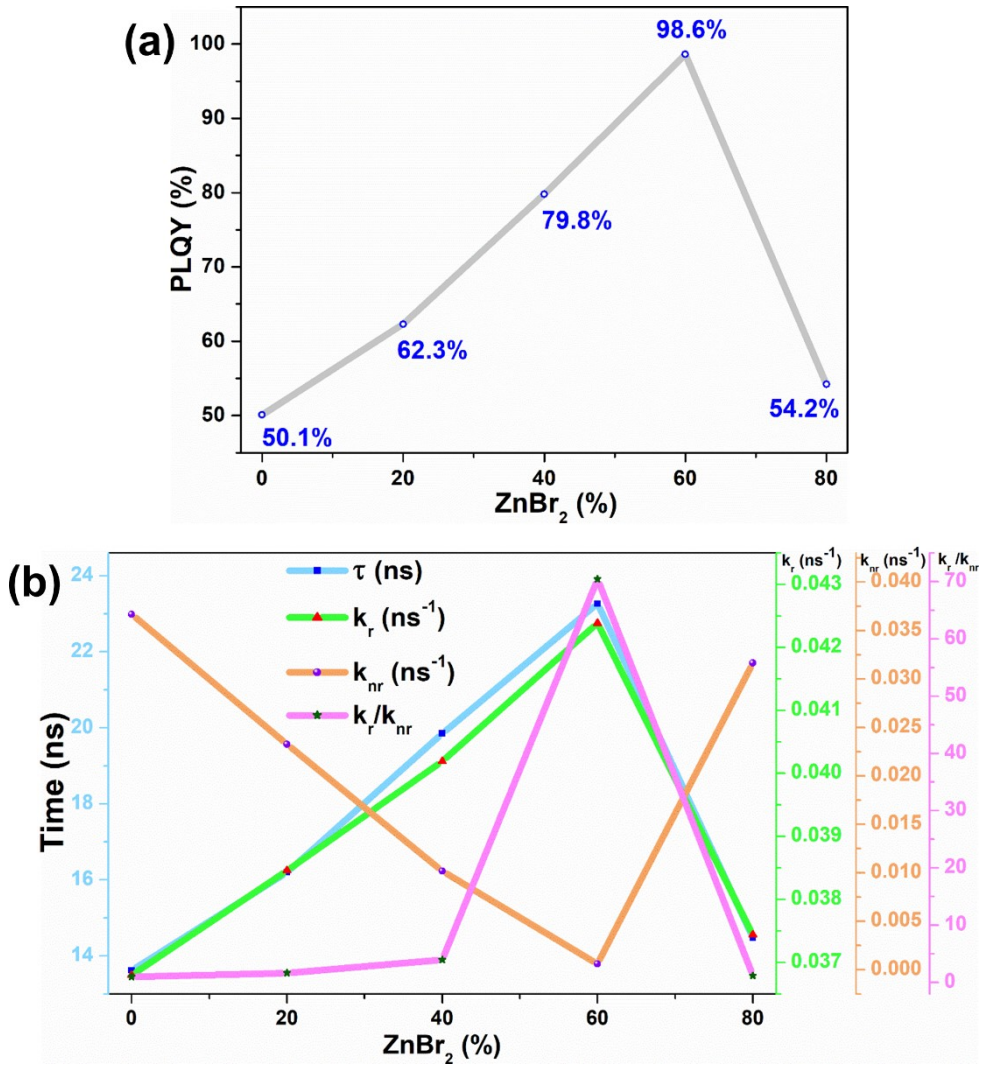

Fig. S5. (a) PLQY, (b) lifetime (τ), k_r, k_{nr}, and k_r/k_{nr} as a function of $ZnBr_2$ doping concentration in $CsPbBr_3$ PNCs.

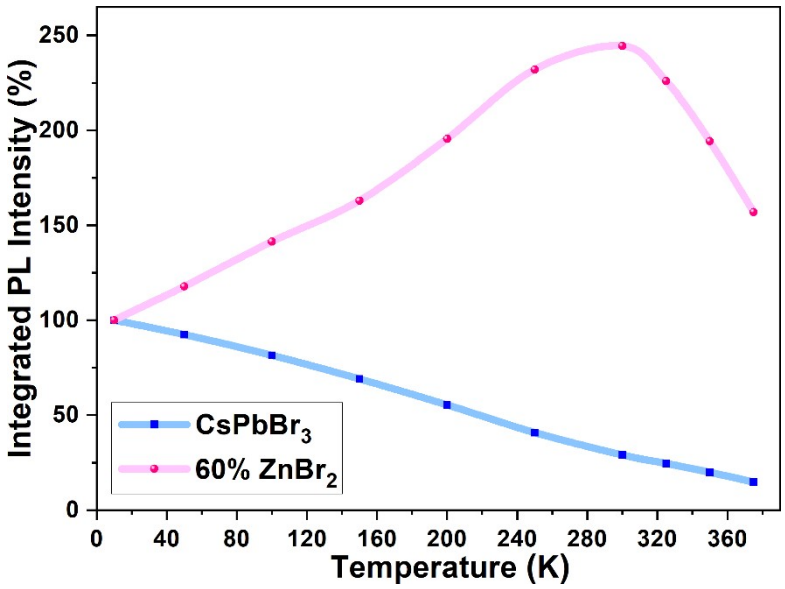

Fig. S6. The relationship between temperature and integrated PL intensities for both $CsPbBr_3$ and $ZnBr_2$ doped PNCs.

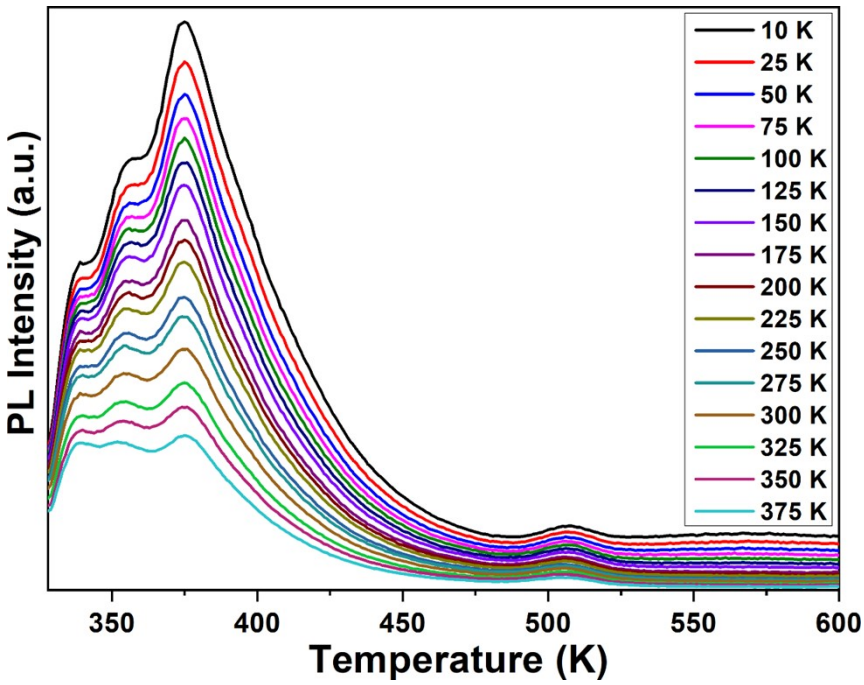

Fig. S7. Temperature-dependent PL spectra of fully transformed Cs_4PbBr_6 PNCs after doping 96% $ZnBr_2$ into $CsPbBr_3$ PNCs.

Calculation of exciton binding energy (BE):

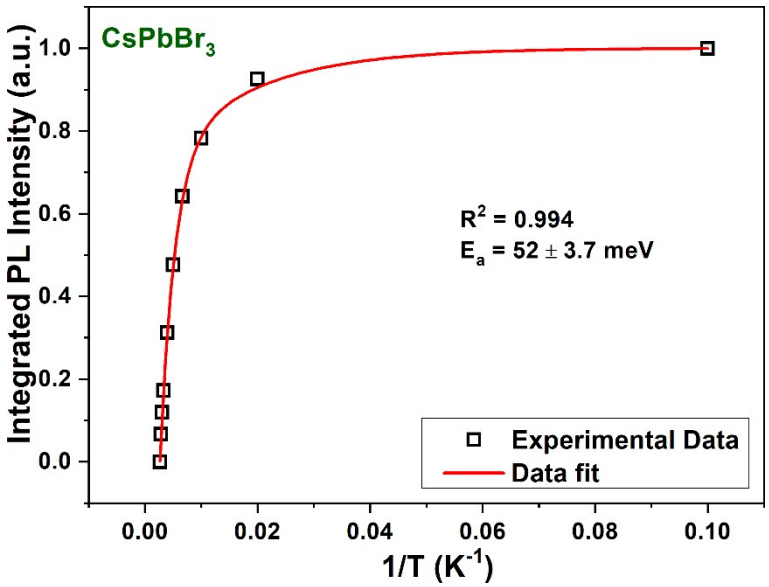

Fig. S8. Integrated PL intensity of pure $CsPbBr_3$ PNCs *vs.* inverse temperature (the solid fitting line is Arrhenius fit for the function: $I_T = \frac{I_o}{1 + C\exp\left(\frac{E_a}{k_B T}\right)}$).

As seen Fig. 6a,b, the integrated PL intensities for pure $CsPbBr_3$ PNCs decreases with increasing the temperature to 375 K, indicating thermal quenching emission. In contrary, the PL intensities of $ZnBr_2$-doped $CsPbBr_3$ increased in the same temperature range, exhibiting negative thermal quenching, owing to suppression of nonradiative carrier trapping centers and introduction of shallow energy levels facilitating radiative recombination process enabling $ZnBr_2$-doped $CsPbBr_3$ PNCs highly luminescent. The PL intensities as a function of temperature were fitted as shown in Fig. S8 for pure $CsPbBr_3$ PNCs, by employing Arrhenius equation **[S5, S6]**:

$$I_T = \frac{I_o}{1 + C\exp\left(\frac{E_a}{k_B T}\right)}, \qquad \text{(S1)}$$

, where I_o is the initial emission intensity at 0 K, I_T is the emission intensity at different temperatures, C is a proportionality constant, and k_B is the Boltzmann constant (8.62×10^{-5} eV K^{-1}). E_a is derived from the integrated PL intensity vs. inverse temperature plots shown in Fig. 8a,b. The best curve fit provided E_a values of 52 ± 3.7 meV for $CsPbBr_3$ PNCs.

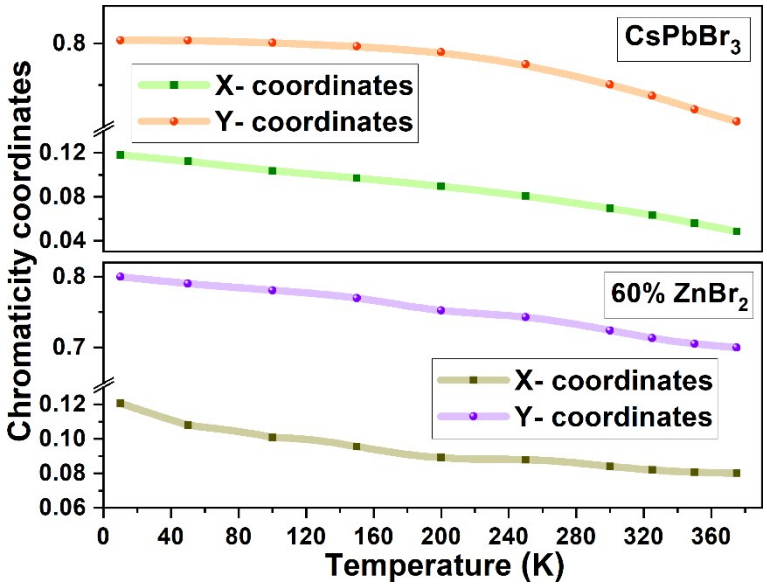

Fig. S9. Relation between color coordinates of pristine and 60% $ZnBr_2$ doped PNCs at various temperatures.

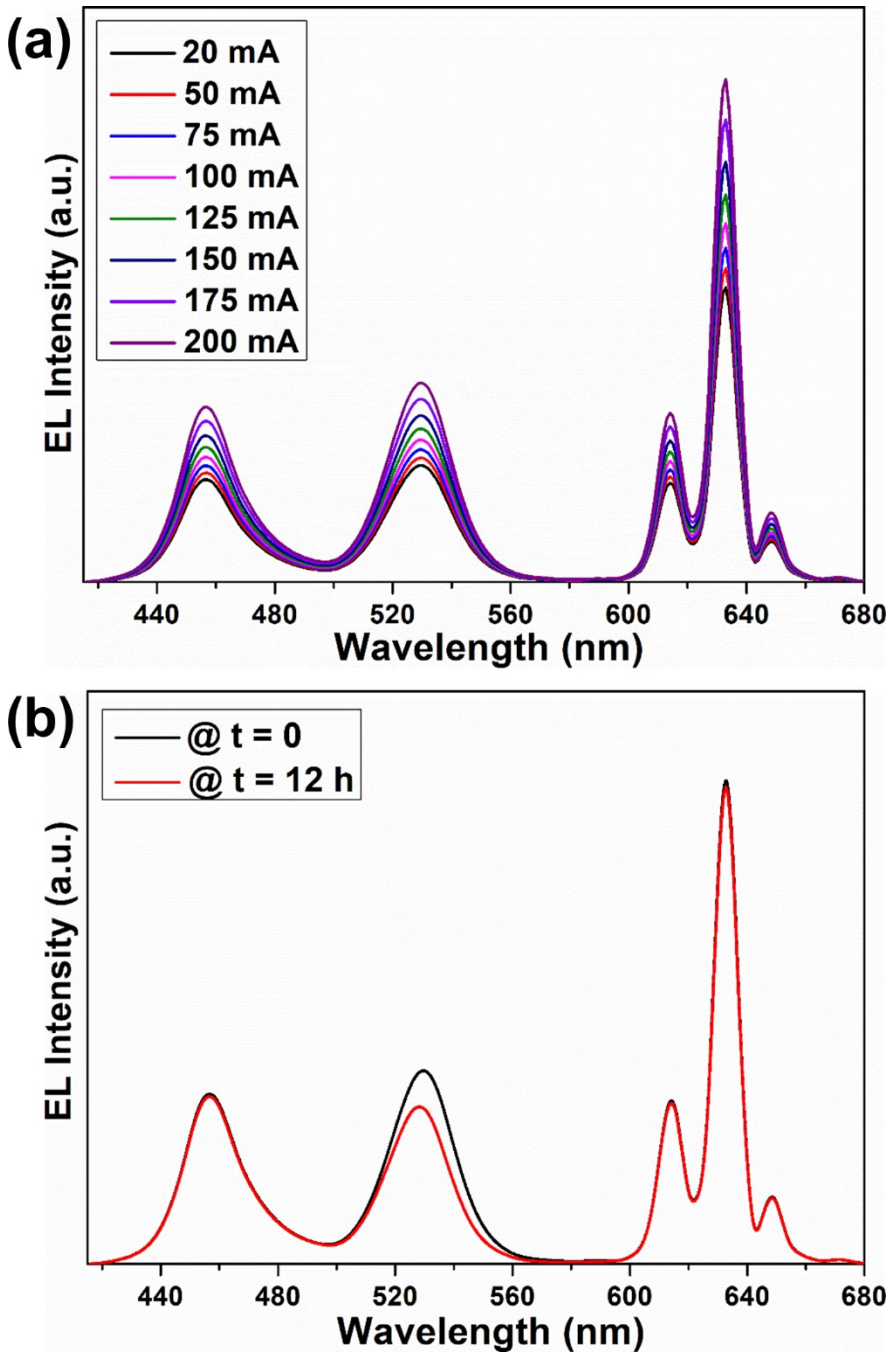

Fig. S10. The EL spectra were measured for the designed WLED device at (a) different operating currents (20-200 mA), and (b) time intervals (0 and 12 h).

References

[S1] Z. Zhao, M. Zhong, W. Zhou, Y. Peng, Y. Yin, D. Tang, B. Zou, *J. Phys. Chem. C*, 2019, **123**, 25349–25358.

[S2] J.H. Cha, J. H. Han, W. Yin, C. Park, Y. Park, T.K. Ahn, J.H. Cho, D.Y. Jung, *J. Phys. Chem. Lett.*, 2017, **8**, 565–570.

[S3] Z. Qin, S. Dai, V.G. Hadjiev, C. Wang, L. Xie, Y. Ni, C. Wu, G. Yang, S. Chen, L. Deng, Q. Yu, G. Feng, Z. Wang, J. Bao, *Chem. Mater.*, 2019, **31**, 9098–9104.

[S4] J.I. Jana, R. Muydinov, P. Rosado, H. Mirhosseini, M. Chugh, O. Nazarenko, D.N. Dirin, D. Heinrich, M.R. Wagner, T.D. Kuhne, B. Szyszka, M.V. Kovalenko, A. Hoffmann, *Phys. Chem. Chem. Phys*., 2020, **22**, 5604–5614.

[S5] V. Naresh, T. Jang, Y. Pang, N. Lee, *Nanoscale*, 2022, **14**, 17789.

[S6] A. Singh, P. Dey, A. Kumari, M.K. Sikdar, P.K. Sahoo, R. Das, T. Maiti, *Phys. Chem. Chem. Phys.,* 2022, **24**, 4065.